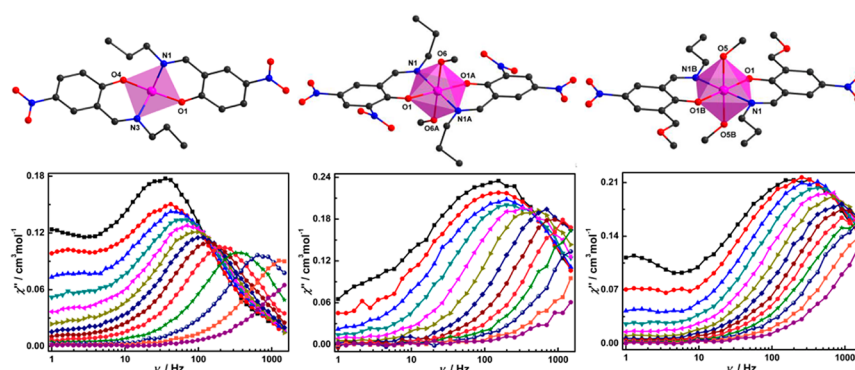


Tuning the Coordination Geometry and Magnetic Relaxation of Co(II) Single-Ion Magnets by Varying the Ligand Substitutions

Guo Peng,* Yu-Feng Qian, Zhi-Wen Wang, Yue Chen, Twinkle Yadav, Karin Fink,* and Xiao-Ming Ren*



ABSTRACT: Three mononuclear Co(II) complexes with the formulas of $[\text{Co}(\text{L}_1)_2]$ (**1**), $[\text{Co}(\text{L}_2)_2(\text{CH}_3\text{OH})_2]$ (**2**), and $[\text{Co}(\text{L}_3)_2(\text{CH}_3\text{OH})_2]$ (**3**) ($\text{HL}_1 = 4$ nitro 2 (*E*) (propylimino)methyl)phenol, $\text{HL}_2 = 2,4$ dinitro 6 (*E*) (propylimino)methyl)phenol, $\text{HL}_3 = 2$ (methoxymethyl) 4 nitro 6 (*E*) (propylimino)methyl)phenol) have been synthesized and structurally characterized. The CH_2OCH_3 group in the ligand of complex **3** was *in situ* formed during the reaction. The Co(II) ion of complex **1** is in a distorted tetrahedral environment, while the Co(II) centers in complexes **2** and **3** adopt a deformed octahedral geometry. The static magnetic data can be well fitted by the spin (1) or Griffith Figgis (2 and 3) Hamiltonian and negative D and B_2^0 values were obtained. Quantum chemical calculations confirm the presence of significant easy axial magnetic anisotropy with non negligible transversal contributions in all the three complexes. All the three complexes show field induced slow magnetic relaxation with one (**2**) or two (**1** and **3**) relaxation processes. Interestingly, their coordination geometry and magnetic relaxation behaviors can be tuned by ligand substitutions.

INTRODUCTION

Extensive research efforts have focused on single molecule magnets (SMMs) in the past three decades, not only because of the unique physics of SMMs^{1–3} but also owing to their potential applications in ultrahigh density information storage, quantum computation, and molecular spintronics.^{4–7} The magnetic properties of SMMs consumedly rely on spin ground state (S) and magnetic anisotropy (D), and the interplay of these two parameters can create an energy barrier (U) to impede spin reversal ($U = DS^2$ for an integer S or $U = D(S^2 - 1/4)$ for a half integer S). To improve the SMM behavior, originally, much attention was paid to the synthesis of polynuclear complexes with a large spin ground state.^{8,9} However, it was found that increasing the nuclearity to enlarge the spin values does not guarantee an optimization of SMM behavior.^{10,11} Thus, exploration has been turned to mono nuclear complexes with considerable anisotropy.^{12–14} Mono nuclear complexes with magnetic bistabilities are also named as single ion magnets (SIMs). Since the discovery of the first

SIM,¹² a large number of SIMs with one lanthanide,^{15–19} transition metal,^{20–23} or actinides ion²⁴ as the spin center have been reported. Impressive progress has been made for SIMs containing Dy(III)^{25–29} or Co(II) ions.^{30–36} The blocking temperature, below which a hysteresis loop shows up, has exceeded liquid nitrogen temperature for the best Dy(III) SIM,³⁷ while the highest energy barrier of Co(II) SIM has reached 450 cm^{-1} .³⁸

Among the documented transition metal SIMs, the most popular are undoubtedly those with Co(II) ions due to their half integer spin ground state and significant magnetic anisotropy from the unquenched spin–orbital couplings,

which can diminish the quantum tunneling of magnetization (QTM) effects and lead to favorable SIM behavior. The magnetic relaxation behavior of Co(II) SIMs is governed by magnetic anisotropy, which is strongly dependent on ligand field strength and coordination geometry. Several strategies such as decreasing coordination number,^{30,38} changing coordination atom,^{39–43} introduction of heavier coordination atom,^{44–48} varying the counteranions,^{49,50} and ligand substitution^{51–59} have been successfully employed to tune the magnetic anisotropy and magnetic properties of Co(II) SIMs. By ligand substitution, the symmetry of the coordination geometry can be changed while the coordination atoms stay the same. This provides an effective avenue to manipulate the magnetic anisotropy and investigate the magneto structural correlations of Co(II) SIMs.

Recently, we have reported two typical Co(II) SIMs with bulky Schiff base ligand, and their structural distortion and magnetic relaxation can be modulated by ligand substitution.⁶⁰ To further study the ligand substitution effects and explore the magneto structural relationship of Co(II) SIMs, three Co(II) complexes, [Co(L₁)₂] (**1**), [Co(L₂)₂(CH₃OH)₂] (**2**), and [Co(L₃)₂(CH₃OH)₂] (**3**) (HL₁ = 4 nitro 2 ((*E*) (propylimino)methyl)phenol, HL₂ = 2,4 dinitro 6 ((*E*) (propylimino) methyl)phenol, HL₃ = 2 (methoxymethyl) 4 nitro 6 ((*E*) (propylimino)methyl)phenol), with different derivatives of Schiff base ligands were synthesized and characterized by structure determination, magnetic investigations and *ab initio* calculations.

EXPERIMENTAL SECTION

General Materials and Methods. All chemicals were commercially available and were used as received without further purification. Elemental analyses (C, H, and N) were conducted on an Elementar vario EL cube elemental analyzer. Fourier transform infrared (IR) spectra were measured on a Nicolet IS10 Spectrum with samples prepared as KBr discs. Powder X ray diffraction (PXRD) patterns were recorded at room temperature on a Bruker D8 Advance diffractometer. Direct current (dc) magnetic measurements were carried out on a Quantum Design PPMS DynaCool 9 magnetometer. The magnetic data were corrected for diamagnetic contribution by using Pascal's constants. Altering current (ac) magnetic measurements were performed on a Quantum Design MPMS XL7 SQUID magnetometer.

Synthesis of [Co(L₁)₂] (L₁ = 4-nitro-2-((*E*)-(propylimino)methyl)phenol) (1**).** 5 Nitrosalicylaldehyde (0.0836 g, 0.5 mmol) and propylamine (42 μ L, 0.5 mmol) were dissolved in a mixture of CH₃OH (10 mL) and C₂H₅OH (10 mL), followed by the addition of Co(CH₃COO)₂·4H₂O (0.0623 g, 0.25 mmol). The resulting mixture was stirred for 25 min at room temperature and then filtered. Slow evaporation of the filtrate produced dark red crystals after several days. Yield: 36 mg (30% based on Co). Calc. (%) for C₂₀H₂₂CoN₄O₆: C 50.75, H 4.68, N 11.84. Found: C 50.82, H 4.70, N 11.88. Selected IR data (cm⁻¹): 2962w, 1623w, 1597w, 1551w, 1495w, 1468w, 1396w, 1311s, 1188w, 1102w, 1054w, 949w, 850w, 707w, 659w 506w, 464w (Figure S1a).

Synthesis of [Co(L₂)₂(CH₃OH)₂] (L₂ = 2,4-dinitro-6-((*E*)-(propylimino)methyl)phenol) (2**).** A CH₃OH (20 mL) solution of 3,5 dinitrosalicylaldehyde (0.1061 g, 0.5 mmol), propylamine (42 μ L, 0.5 mmol), and Co(CH₃COO)₂·4H₂O (0.0623 g, 0.25 mmol) was stirred for 30 min at room temperature and then filtered. Slow evaporation of the filtrate produced red crystals after several days. Yield: 67 mg (43% based on Co). Calc. (%) for C₂₂H₂₈CoN₆O₁₂: C 42.11, H 4.50, N 13.39. Found: C 41.84, H 4.37, N 13.58. Selected IR data (cm⁻¹): 3443w, 2973w, 1637w, 1596w, 1565w, 1527m, 1491w, 1461w, 1437w, 1330s, 1305m, 1227w, 1103w, 1012w, 921w, 842w, 790w, 709w, 634w, 526w, 439w (Figure S1b).

Synthesis of [Co(L₃)₂(CH₃OH)₂] (L₃ = 2-(methoxymethyl)-4-nitro-6-((*E*)-(propylimino) methyl)phenol) (3**).** A CH₃OH (20 mL) solution of 3 chloromethyl 5 nitrosalicylaldehyde (0.1078 g, 0.5 mmol) and propylamine (42 μ L, 0.5 mmol) was stirred for 10 min at room temperature, followed by the addition of Co(CH₃COO)₂·4H₂O (0.0623 g, 0.25 mmol). The resulting mixture was stirred for another 20 min and then filtered. Slow evaporation of the filtrate produced brown crystals after several days. Yield: 54 mg (34% based on Co). Calc. (%) for C₂₆H₃₈CoN₄O₁₀·0.5H₂O: C 49.21, H 6.20, N 8.83. Found: C 49.16, H 5.87, N 8.74. Selected IR data (cm⁻¹): 3318w, 2960w, 2872w, 1633w, 1599w, 1568w, 1489w, 1304s, 1286s, 1102m, 1023w, 954w, 908w, 833w, 775w, 715w, 611w, 517w, 482w (Figure S1c).

Computational Details. All calculations on complexes **1–3** are based on the respective X ray structures. The positions of the hydrogen atoms were reoptimized with density functional calculations (BP86 functional/def SVP basis set) with the Turbomole program package.⁶¹ On the basis of these structures, the basis sets of Co, O, and N were extended to def2 TZVP. The state average complete active space self consistent field (CASSCF) calculations taking into account all quartet states with seven electrons in the five 3d orbitals were performed.⁶² On the basis of the CASSCF orbitals, spin orbit configuration interaction (SOC) calculations were performed with a program developed in Karlsruhe and Kaiserslautern,^{63,64} using a spin-orbit mean field approach for the 2 electron spin-orbit integrals.^{65,66} *g* tensors were obtained by the Abragam–Bleaney tensor as described by Gerloch and McMeeking;⁶⁷ magnetic susceptibilities were calculated by Boltzman averaging from the derivatives of the energy with respect to the magnetic field.

Crystal Structure Determination and Refinement. The single crystal diffraction data of **1–3** were collected at 173(2)–175(2) K on a Bruker APEX II diffractometer with monochromated Mo- α radiation ($\lambda = 0.71073$ Å). The sorption corrections were conducted using TWINABS for **1** and SADABS for **2** and **3** supplied by Bruker. The structures were solved by direct methods and refined by full matrix least squares analysis on *F*², using the SHELXTL program package.⁶⁸ The structure of **1** was refined as a two component twin, and some carbon atoms were found to be disorder in the structure of **3**. Ordered non H atoms were refined anisotropically, H atoms were placed in calculated positions and refined using a riding model. The data have been deposited to the Cambridge Crystallographic Data Centre with CCDC 2019087–2019089. Data collection and structural refinement parameters are listed in Table 1.

RESULTS AND DISCUSSION

Synthesis and General Characterization. The reactions of substituted salicylaldehyde, propylamine, and Co (CH₃COO)₂·4H₂O in the presence of organic solvent (methanol or a mixture of methanol and ethanol) in one pot afforded crystals **1–3** (Scheme 1). Complex **1** could also be obtained when the reaction was made in amethanol solution, but the yield was very low. The CH₂OCH₃ group in the ligand of complex **3** was *in situ* formed during the reaction, and similar reactions can also be found in the literature.^{69,70} Attempts to synthesize the diamagnetic Zn or Mg analogues of complex **1** were unsuccessful. The experimental PXRD patterns of all the three complexes are in accordance with those from simulations based on crystallographic data (Figure S2), confirming the phase purity and stability of the bulk sample of as synthesized products.

Structure Analysis. Single crystal diffractions demonstrate that all the three complexes crystallize in a triclinic system with the space group *P1*. There are one Co(II) ion and two ligands in the asymmetry unit of **1** (Figure 1a). The Co(II) center coordinates to two singly deprotonated ligands adopting a distorted tetrahedral CoN₂O₂ coordination environment. The

Table 1. Crystallographic Data and Structure Refinement for Complexes 1–3

	1	2	3
formula	C ₂₀ H ₂₂ CoN ₄ O ₆	C ₂₂ H ₂₈ CoN ₆ O ₁₂	C ₂₆ H ₃₈ CoN ₄ O ₁₀
M _r (g mol ⁻¹)	473.34	627.43	625.53
crystal system	triclinic	triclinic	triclinic
space group	$P\bar{1}$	$P\bar{1}$	$P\bar{1}$
T (K)	175(2)	173(2)	173(2)
a (Å)	9.4970(6)	7.8713(6)	8.5595(8)
b (Å)	10.5464(7)	8.3674(6)	8.7955(9)
c (Å)	11.9011(7)	10.6989(7)	10.7634(12)
α (deg)	113.022(2)	98.280(2)	97.263(4)
β (deg)	94.458(2)	106.406(2)	112.277(4)
γ (deg)	105.003(2)	95.001(3)	99.250(3)
V (Å ³)	1037.97(11)	662.82(8)	724.35(13)
Z	2	1	1
D _c (g cm ⁻³)	1.515	1.572	1.434
μ (mm ⁻¹)	0.872	0.722	0.654
F(000)	490	325	329
reflections collected		5465	6289
unique reflections	3587	2405	2521
R _{int}		0.0397	0.0620
GOF	1.054	1.066	1.054
R ₁ (I > 2σ)	0.0513	0.0411	0.0622
wR ₂ (all data)	0.1317	0.0867	0.1488
max. diff. peak/hole (e Å ⁻³)	0.453/ 0.360	0.308/ 0.315	0.330/ 0.529

dihedral angle between the two chelate planes fabricated by Co–N–C–C–O is 70.67°, which is smaller than those of other Co(II) complexes with tetrahedral geometry.^{52–54} The Co–N and Co–O bond lengths fall in the range 1.906(3)–1.985(4) Å, and the Co–N bond distances are longer than those of Co–O. The bond angles around the Co(II) center vary from 95.78(15)° to 136.81(12)°, all of which deviate from 109.5° for an perfect tetrahedron. The O–Co–N angles within one of the ligands are similar and close to 96°. To further evaluate the distortion of coordination geometry, continuous

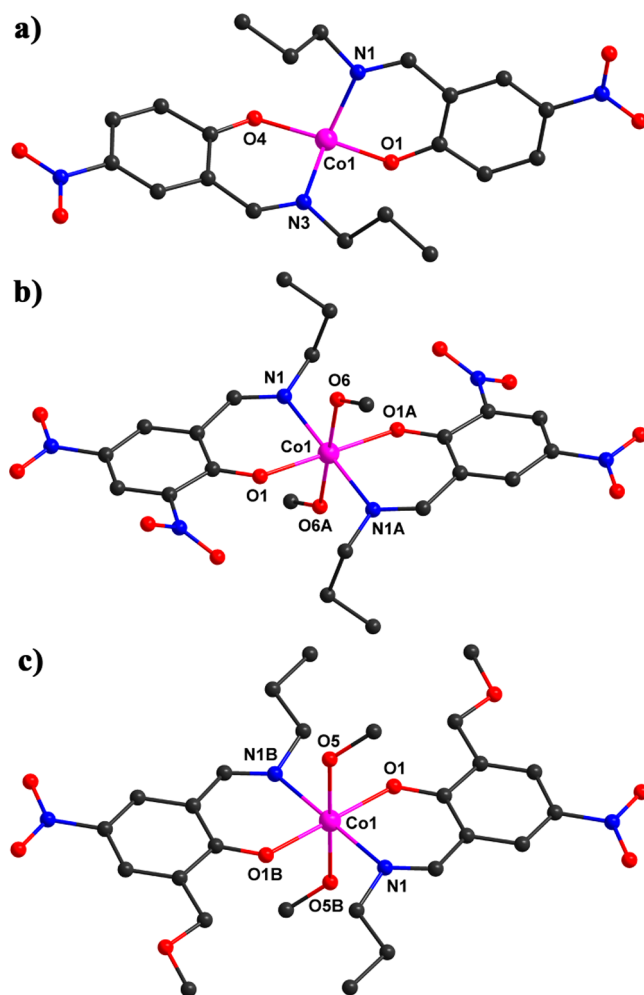
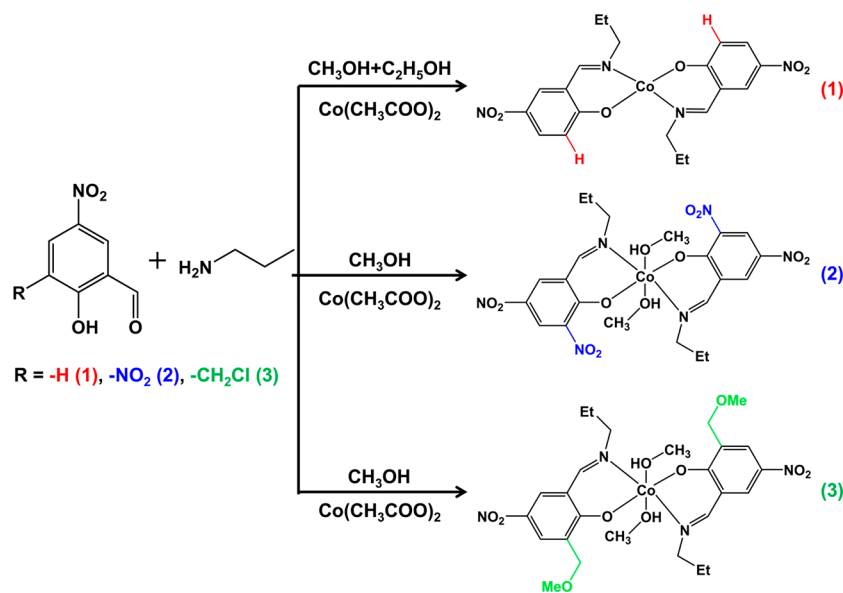


Figure 1. (a–c) Structures of 1–3. Symmetry codes: A 1 – x, –y, 1 – z; B 2 – x, 1 – y, –z.

shape measures (CShMs)^{71,72} were conducted for 1. This results in a CShM value of 3.223 (Table S1), indicating that

Scheme 1. Synthetic Route for Complexes 1–3



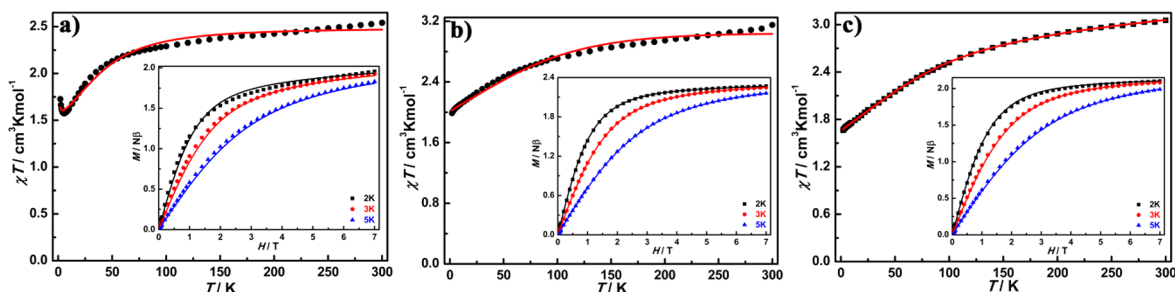


Figure 2. (a–c) Temperature dependence of the χT products for complexes 1–3. Inset: Field dependent magnetization plots below 5 K. The solid lines are the best fit curves by the spin (a) or Griffith–Figgis (b and c) Hamiltonian.

the coordination geometry of **1** exhibits relatively large deviation from an ideal tetrahedron. The nearest intermolecular Co...Co distance is 6.4311(9) Å.

The molecular structures of **2** and **3** are similar except the groups in the second position of the ligands. The second position of the ligand for **2** is occupied by a NO₂ group, whereas the same place for **3** is taken by a CH₂OCH₃ group (Scheme 1). The structures of **2** and **3** contain one Co(II) ion, two ligands, and two coordinated methanol molecules (Figure 1b,c). The Co(II) ions coordinate to two nitrogen atoms and four oxygen donors from two ligands and two methanol molecules. The coordination geometry of Co(II) centers can be described as a distorted octahedron, which is verified by continuous shape measures with CShM values of 0.181 for **2** and 0.100 for **3**, respectively (Table S1). The relatively small CShM value suggests that the coordination geometry of **3** is more close to a perfect octahedron. The oxygen atoms from phenol groups locate at axial position, while the equatorial sites are occupied by two nitrogen and two oxygen donors from two ligands and two methanol molecules. The axial Co–O bond lengths (2.0316(16) Å for **2** and 2.025(3) Å for **3**) are shorter than the equatorial Co–O/N (2.1804(18) and 2.117(2) Å for **2** and 2.125(3) and 2.126(4) Å for **3**) bond distances, indicating that the coordination polyhedrons of **2** and **3** are compressed along the O(phenol)–Co–O(phenol) bond. The axial O–Co–O bond angles are equal to 180°, whereas the equatorial O–Co–N bond angles are in the range 88.02(14)°–91.99(14)°. The closest intermolecular Co...Co separations are 7.8713(6) Å for **2** and 8.5595(8) Å for **3**, respectively.

Although the coordination polyhedrons of **2** and **3** can be geometrically assigned to compressed octahedron, it should be considered that the average values of Co–O and Co–N bond lengths are different in octahedral complexes. The deviations of the bond lengths from their average values ($d_i = R_i - R_{\text{avg}}$) are crucial and produce the structural distortion parameter ($d_{\text{str}} = d_{\text{ax}} - d_{\text{eq}}$). Positive d_{str} values for **2** and **3** were obtained on the basis of the viewpoints and values given by Titiš and Boča (Table S2),⁷³ suggesting that the electronic behavior of these two complexes correspond to that of an elongated tetragonal bipyramid taking the methanol oxygens as axial ligands. In such cases, first order spin–orbit coupling has to be involved to describe the magnetic properties of the resulting compounds, which is consistent with the conclusions from the magnetic studies and the theoretical calculations (see below).

Static Magnetic Studies. Magnetic susceptibility measurements were performed on polycrystalline samples of **1–3** in the temperature range 2–300 K under a 1000 Oe static field. The χT products of **1–3** at 300 K are 2.54, 3.15, and 3.05 cm³ K mol⁻¹, respectively (Figure 2). Their values are higher than

the spin only value of 1.875 cm³ K mol⁻¹ for a high spin Co(II) ion with $S = 3/2$ and $g = 2$, suggesting the existence of unquenched orbital contributions to the magnetic moment. The χT value of **1** gradually decreases with cooling to a minimum of 1.57 cm³ K mol⁻¹ at 5.5 K and then suddenly increases to 1.73 cm³ K mol⁻¹ at 2 K, whereas the χT products of **2** and **3** monotonously decrease with reduction of temperature and reach 1.99 and 1.66 cm³ K mol⁻¹ at 2 K, respectively. The decrease is probably due to the thermal depopulation of higher energy Kramers doublets of the Co(II) ion or/and the antiferromagnetic couplings between different monomers, whereas the increase observed in **1** below 5.5 K indicates the presence of weak intermolecular ferromagnetic interactions between neighboring Co(II) ions. The field dependences of the magnetization below 5 K for **1–3** increase with a lifting magnetic field, and the magnetizations reach 1.96, 2.27, and 2.10 N β (N and β are Avogadro constant and Bohr magneton), respectively. These values are lower than the saturation magnetization of 3 N β for a high spin Co(II) ion with $S = 3/2$ and $g = 2$. The lack of saturation and the observation of nonoverlapping isothermal magnetization curves imply the existence of considerable magnetic anisotropy.

To get more information about the magnetic anisotropy, the magnetic data of **1** was analyzed by the zero field splitting (ZFS) Hamiltonian in eq 1 using the program PHI⁷⁴

$$\hat{H} = D[\hat{S}_z^2 - S(S+1)/3] + E(\hat{S}_x^2 - \hat{S}_y^2) + \beta g \hat{S}H \quad (1)$$

in which D and E are the axial and rhombic ZFS parameters, S is the spin operator, β is the Bohr magneton, g is Landé factor, and H is the magnetic field vector, respectively. The best fits gave parameters $D = -49.9$ cm⁻¹, $E = 6.3$ cm⁻¹, and $g_{\text{iso}} = 2.30$ and intermolecular interactions $zj = 0.026$ cm⁻¹ (Figure 2a). The large and negative D value indicates the presence of strong easy axis magnetic anisotropy in **1**. No reasonable results could be obtained when a positive D value was used.

Attempts to fit the magnetic data of **2** and **3** with ZFS model were unsuccessful. This is likely ascribed to the strong first order spin–orbital coupling (SOC) presented in Co(II) complexes with octahedral geometry; the ZFS parameters D and E are no longer appropriate for modeling the magnetic properties of **2** and **3**. Therefore, the magnetic data of **2** and **3** were fitted by the Griffith–Figgis Hamiltonian, which explicitly considers first order SOC given in eq 2:

$$\hat{H} = -\alpha \lambda \hat{L}_{\text{Co}} \hat{S}_{\text{Co}} + \alpha^2 B_2^0 [3\hat{L}_{z,\text{Co}}^2 - \hat{L}^2] + \beta H(-\alpha \hat{L}_{\text{Co}} + g_e \hat{S}_{\text{Co}}) \quad (2)$$

where λ is the SOC parameter, α is an orbital reduction factor, and B_2^0 represents a crystal field parameter for an axial

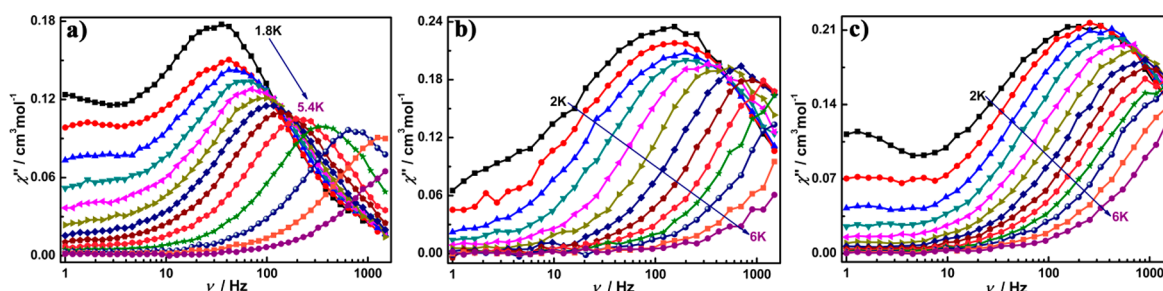


Figure 3. (a–c) Frequency dependence of out of phase ac susceptibility data under a 2000/1000/1500 Oe dc field for 1–3.

distortion. The best fit of the magnetic data with PHI program⁷⁴ results in $\alpha = 1.33$, $\lambda = -164 \text{ cm}^{-1}$, $B_2^0 = -201.7 \text{ cm}^{-1}$, $\text{TIP} = 2.73 \times 10^{-4} \text{ cm}^3 \text{ cm}^{-1}$ for 2 and $\alpha = 0.94$, $\lambda = -197 \text{ cm}^{-1}$, $B_2^0 = -273.6 \text{ cm}^{-1}$, $\text{TIP} = 1.67 \times 10^{-3} \text{ cm}^3 \text{ cm}^{-1}$ for 3 (Figure 2b,c). The large and negative B_2^0 values imply the presence of strong axial magnetic anisotropy in 2 and 3. These values are comparable to those found in other Co(II) complexes with distorted octahedral coordination geometry.^{75–77} Worse results were obtained when positive B_2^0 values were employed.

Quantum Chemical Calculation. In order to get information about the electronic states and the magnetic anisotropy, complete active space self consistent field (CASSCF) and spin–orbit configuration interaction (SOC) calculations based on the crystal structures were performed for all the complexes. The details of the calculations are presented in the Experimental Section. The CASSCF calculations provide information about the ligand field. The splitting of the 4F state of the free Co(II) ion is shown in Table S3. The ground state of complex 1 is separated from the two next states by 1941 and 3674 cm^{-1} , respectively, whereas the energy gaps between the first three quartet states of 2 and 3 are relatively small and these three states can be considered as quasi degenerate. The lowest doublet states are found at the energies of 15741 cm^{-1} for 1, 13310 cm^{-1} for 2, and 12979 cm^{-1} for 3, respectively. They are well separated from the lowest three quartet states and do not play an important role in the SOC calculations. The results of the SOC calculations are presented in Table S4. The contributions of the first three quartet states obtained in the CASSCF calculations to the lowest six Kramer’s doublets are shown in Tables S5–S7. For most of these Kramer doublets, the three quartet states cover more than 99% of the wave function. The contribution of the different M_s values is summarized in Tables S8–S10. As expected from the distorted tetrahedral coordination as well as from the isolated quartet ground state in the CASSCF calculation, complex 1 shows a second order behavior of the spin–orbit coupling. The first quartet state is split into two Kramer’s doublets with an energy difference of 76 cm^{-1} . The wave functions of these two Kramer doublets are dominated by the components of the first quartet state, which contributes with 94% and 98%, respectively. Analyzing the wave functions with a pseudo spin of $S = 3/2$ yields $D = -36.4 \text{ cm}^{-1}$, $E = 6.3 \text{ cm}^{-1}$, $g_x = 2.278$, $g_y = 2.109$, and $g_z = 2.609$ for 1. The sign of D is also confirmed by the g values obtained individually for the first and second Kramer doublets (Table S11) and are consistent with the fitting of the magnetic data. Both theoretical and experimental D values are negative, verifying the presence of easy axis magnetic anisotropy in 1. The calculated χT versus T plot (Figure S3) can reproduce the measured data reasonably well,

taking into account that intermolecular interactions are not included.

Complexes 2 and 3 possess distorted octahedral structures. This is in agreement with the quasi degeneracy of the first three quartet states in the CASSCF calculations. These three quartet states strongly interact in the SOC calculations, resulting in six Kramer’s doublets in a range of 1500 cm^{-1} . In agreement with the smaller deviation from octahedral symmetry and the lower energies of the second and third quartet states in the CASSCF calculations, the second Kramer doublet is found at higher energies in complex 3. This is supported by the stronger contribution of the second quartet state to the wave functions in complex 3 (38% in complex 3 and 22% in complex 2, respectively). Again, the calculated magnetic susceptibilities are in reasonable agreement with the experiment (Figure S3). The g_z values of the first Kramer doublet for 2 and 3 are much larger than those of g_x and g_y , confirming that an easy axis type of magnetic anisotropy can be also found in 2 and 3 (Table S11). This is in line with the observation of negative B_2^0 values in the fitted results. The relatively large effective g_x and g_y values suggest that the transversal anisotropy and quantum tunneling of magnetization (QTM) effects in complexes 1–3 are non negligible. The magnetic axes in complexes 1–3 are shown in Figure S4.

Dynamic Magnetic Investigations. In view of the remarkable magnetic anisotropy in complexes 1–3, ac susceptibility measurements were conducted to explore their magnetic dynamics. No out of phase ac signals were observed for all the three complexes in the absence of a dc field, which is probably ascribed to the influence of QTM. However, the out of phase ac signals of these complexes can be switched on by the application of various dc fields (Figures S5–S7). The magnetic relaxations are slowest at 2000, 1000, and 1500 Oe for 1–3, respectively. Therefore, the frequency dependence of ac susceptibility at different temperatures was further investigated under these optimal fields. This leads to significant out of phase ac signals with clear maxima (Figure 3 and Figure S8), suggesting that all the three complexes are field induced SIMs. Two relaxation processes were observed in 1 and 3, whereas only one relaxation pathway was detected in 2. The peaks of out of phase components can be observed in the ranges 1.8–5.1 K for 1, 2–4.4 K for 2, and 2–4.4 K for 3 in the frequency range 1–1488 Hz (Figure 3).

The Cole–Cole plots of 1–3 can be modeled by a modified/generalized Debye function (see eqs S1–S4 in the Supporting Information) using the CC FIT program (Figure 4a–c).⁷⁸ The fits result in $\alpha_1 = 0.033$ –0.16 and $\alpha_2 = 0$ –0.23 for 1, $\alpha = 0.019$ –0.44 for 2, and $\alpha_1 = 0.075$ –0.38 and $\alpha_2 = 0$ for 3 (Tables S12–S14). The presence of more than one α value in a compound and the observation of relatively large α

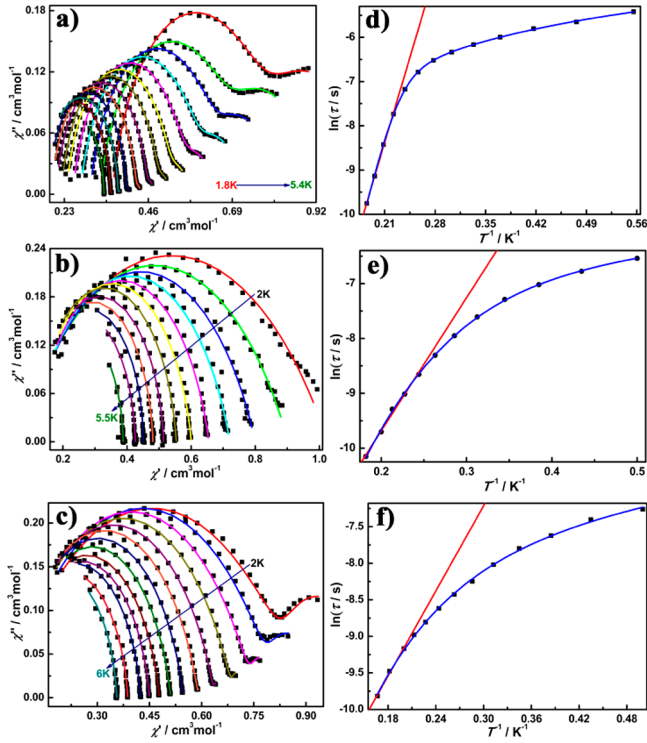


Figure 4. (a–c) Cole–Cole plots for 1–3. The solid lines are the best fits to a modified/generalized Debye model. (d–f) Temperature dependence of the relaxation times under a 2000/1000/1500 Oe dc field for 1–3. The red lines are the best fits to an Arrhenius law (d–f). The blue lines are fits for the sum of Orbach, Raman, and direct processes (d) or Raman plus direct processes (e and f).

values imply that the magnetic relaxations in these systems are realized by multichannels, such as Orbach, Raman, direct, and QTM processes. These processes can be described by eq 3, where the first two terms are Orbach and Raman pathways and the last two terms represent direct and QTM processes. Thermally activated behavior observed in the high temperature range is generally attributed to an Orbach relaxation process, and the energy barrier (U_{eff}) of the Orbach process is expected to be close or equal to the energy gap between real electronic states, whereas the Raman process contains transitions of absorption and re emission of phonons *via* virtual states.²² The presence of other channels, such as Raman, direct, and QTM processes, will decrease the U_{eff} value. The relaxation times obtained from the Cole–Cole plots fitting versus temperature produces Arrhenius curves. The fits by an Arrhenius law to the high temperature data gave the following energy barriers and pre exponential factors: $U_{\text{eff}} = 54.9$ K with $\tau_0 = 2.28 \times 10^{-9}$ s for 1, $U_{\text{eff}} = 24.3$ K with $\tau_0 = 4.89 \times 10^{-7}$ s for 2, and $U_{\text{eff}} = 19.4$ K with $\tau_0 = 2.19 \times 10^{-6}$ s for 3 (Figure 4d–f). The energy barrier of 1 is lower than the calculated energy gap (109.4 K or 76 cm^{-1}) between the lowest two spin–orbit states of the Co(II) ions. However, these two values have the same order of magnitudes, indicating that multiple relaxation processes are involved in this system including the presence of an Orbach process. The fit of the high temperature part of $\ln \tau$ versus $\ln T$ plot results in $n = 11.2$ for 1 (Figure S9a). This value is larger than the Raman exponent for a Kramers ion ($1 < n \leq 9$),^{79–81} further demonstrating that an Orbach process is present in the high temperature range. The relaxation behavior was observed under an applied magnetic field, and no temperature

independent part can be found in the $\ln \tau$ versus T^{-1} plot; therefore, the QTM pathway was considered to be quenched in this system. Therefore, a model including Orbach, Raman, and direct processes (eq 4) was employed to fit the $\ln \tau$ versus T^{-1} plot of 1 in the whole temperature range. The best fit generates the following parameters: $U_{\text{eff}} = 67.1$ K, $\tau_0 = 2.46 \times 10^{-10}$ s, $C = 7.32 \text{ s}^{-1} \text{ K}^{-2.8}$, $n = 2.8$, $A = 105 \text{ s}^{-1} \text{ K}^{-1}$ (Figure 4d). If only Raman and direct processes were used to fit the $\ln \tau$ versus T^{-1} plot in the whole temperature range (Figure S9b), a large n value was obtained ($n = 12.2$). This value is also much larger than the Raman exponent for a Kramers ion ($1 < n \leq 9$),^{79–81} confirming that the magnetic relaxation of 1 in the high temperature region is realized *via* an Orbach process.

The energy barriers of 2 and 3 are far from the theoretical energy gaps (269 K or 187 cm^{-1} for 2 and 396 K or 275 cm^{-1} for 3, Table S4), which suggests the presence of virtual states in the magnetic relaxation pathway and magnetic relaxations in the high temperature range possibly achieved *via* Raman rather than Orbach processes. The fit of the high temperature part of $\ln \tau$ versus $\ln T$ curves leads to $n = 5$ for 2 and $n = 3.3$ for 3 (Figure S10). The n values fall in the normal range for a Raman process ($1 < n \leq 9$ is reasonable for a Raman process).^{79–81} This further confirms that the magnetic relaxation of 2 and 3 in the high temperature region is dominated by a Raman process. The QTM relaxation process was considered to be quenched by an applied magnetic field. Thus, only Raman and direct processes were employed to fit the $\ln \tau$ versus T^{-1} curves of 2 and 3. The $\ln \tau$ versus T^{-1} curves of 2 and 3 in the full temperature range can be reproduced well by considering both Raman and direct processes (eq 5) (Figure 4e,f), leading to $C = 1.17 \text{ s}^{-1} \text{ K}^{-5.8}$, $n = 5.8$, $A = 311.8 \text{ s}^{-1} \text{ K}^{-1}$ for 2 and $C = 8.74 \text{ s}^{-1} \text{ K}^{-4.1}$, $n = 4.1$, $A = 616.4 \text{ s}^{-1} \text{ K}^{-1}$ for 3. This phenomenon verifies that the magnetic relaxation of 2 and 3 are realized by the mixture of Raman and direct processes, which is consistent with other Co(II) SIMs with octahedral geometry.^{82–84}

$$\tau^{-1} = \tau_0^{-1} \exp(-U_{\text{eff}}/k_{\text{B}}T) + CT^n + AT + \tau_{\text{QTM}}^{-1} \quad (3)$$

$$\tau^{-1} = \tau_0^{-1} \exp(-U_{\text{eff}}/k_{\text{B}}T) + CT^n + AT \quad (4)$$

$$\tau^{-1} = CT^n + AT \quad (5)$$

Magneto-Structural Correlation. It was established that the magnetic relaxation of SIMs can be influenced by many factors such as magnetic anisotropy, ligand field strength, symmetry of coordination geometry, intermolecular interaction, and molecular vibration.^{20–23,25,26,38–59,85–88} The substituent of the Schiff based ligand can regulate the coordination symmetry of Co(II) ions and thus lead to a tetrahedral geometry for 1 and octahedral geometries for 2 and 3. Different coordination geometries will produce a distinct electronic structure for the Co(II) ion, which strongly influences the magnetic anisotropy and magnetic relaxation of the resulting products. In the quantum chemical calculations, all the three complexes show significant magnetic anisotropy but their relaxation behavior was observed only under a dc field. This indicates the presence of strong QTM in these systems, which is confirmed by the observation of large g_x and g_y values in the lowest Kramers doublets. The transversal effects in 2 and 3 are much more remarkable than that of 1, and thus, their energy barriers are lower than that of 1. Although the coordination geometries of 2 and 3 are similar, their distortions are different. This leads to distinct energy

separations (544 cm^{-1} for **2** and 127 cm^{-1} for **3**) between the two lowest quartet states, resulting in different SOC and magnetic relaxation behavior. Two relaxation processes were detected in **1** where the nearest Co...Co distance is relatively short. Therefore, the second relaxation process of **1** is from intermolecular dipole–dipole interactions.^{88,89} Though the closest Co...Co separation in **3** is longer than that in **2**, two relaxation processes were observed in **3** and only one relaxation process appeared in **2**. Therefore, it is not clear whether the second relaxation process in **3** is induced by intermolecular interaction. We compared the structures of **2** and **3** carefully and found that there are more C–H bonds in **3**. Thus, the appearance of the additional relaxation process in **3** is probably attributed to intermolecular dipole–dipole interactions induced by the application of a relatively larger dc field (1000 Oe for **2** and 1500 Oe for **3**) or/and the contribution of C–H bond vibrations.^{22,25,26} From the discussion above, the differences in coordination geometry, structural distortion, intermolecular interactions, and/or molecular vibration are the main reasons for the observation of the distinct magnetic relaxation behavior in **1**–**3**.

CONCLUSION

Three mononuclear Co(II) complexes with different derivatives of Schiff base ligand have been prepared and magnetically characterized. The substituent of the Schiff based ligand can regulate the coordination geometry and the distortion of the coordination polyhedrons. Complex **1** holds a tetrahedral coordination geometry, whereas complexes **2** and **3** possess octahedral coordination geometry with different distortions. Magnetic studies and quantum chemical calculations reveal that all three complexes exhibit strong easy axial anisotropy with pronounced transversal contributions. All the three complexes show field induced SIM behavior. The magnetic relaxation of **1** is achieved by Orbach, Raman, and direct processes, whereas Raman and direct processes are dominant in **2** and **3**. This suggests that large and negative D/B_2^0 values do not guarantee the existence of an Orbach process, which is consistent with the behavior observed in other Co(II) SIMs.^{75,83,90,91} Their magnetic relaxation behaviors can not only be manipulated by the coordination geometry and its distortion but also be influenced by intermolecular interactions or/and molecular vibrations. The work presented herein not only extends the family of Co(II) SIMs but also it will direct us to tune and improve the magnetic properties of SIMs by ligand substitution. The employment of other Schiff base ligands with flexible groups to construct new Co(II) SIMs is in progress.

ASSOCIATED CONTENT

Figures of IR spectra, PXRD patterns, χT vs T plots, magnetic axes schematics, ac susceptibility, and $\ln \tau$ vs $\ln T$ plots, tables of continuous shape measures, selected bond distances and distortion parameters, energies of the seven lowest quartet states and the lowest doublet state obtained in the CASSCF calculations, energies of the seven lowest Kramers doublets obtained in the spin orbit CI calculations, contributions of the different M_s components, calculated g tensors, and Cole–Cole parameters, and details of equations (PDF)

Accession Codes

CCDC 2019087–2019089 contain the supplementary crystallographic data for this paper. These data can be obtained free of charge via www.ccdc.cam.ac.uk/data_request/cif, or by emailing data_request@ccdc.cam.ac.uk, or by contacting The Cambridge Crystallographic Data Centre, 12 Union Road, Cambridge CB2 1EZ, UK; fax: + 44 1223 336033.

AUTHOR INFORMATION

Corresponding Authors

Guo Peng – School of Chemistry and Molecular Engineering, Nanjing Tech University, Nanjing 211816, P. R. China; [orcid.org/0000 0002 6604 4546](https://orcid.org/0000-0002-6604-4546); Email: guopeng@njtech.edu.cn

Karin Fink – Institute of Nanotechnology, Karlsruhe Institute of Technology, 76344 Eggenstein Leopoldshafen, Germany; Email: karin.fink@kit.edu

Xiao Ming Ren – School of Chemistry and Molecular Engineering, Nanjing Tech University, Nanjing 211816, P. R. China; [orcid.org/0000 0003 0848 6503](https://orcid.org/0000-0003-0848-6503); Email: xmren@njtech.edu.cn

Authors

Yu Feng Qian – School of Chemistry and Molecular Engineering, Nanjing Tech University, Nanjing 211816, P. R. China

Zhi Wen Wang – School of Chemistry and Molecular Engineering, Nanjing Tech University, Nanjing 211816, P. R. China

Yue Chen – School of Chemistry and Molecular Engineering, Nanjing Tech University, Nanjing 211816, P. R. China

Twinkle Yadav – Institute of Nanotechnology, Karlsruhe Institute of Technology, 76344 Eggenstein Leopoldshafen, Germany

Notes

The authors declare no competing financial interest.

ACKNOWLEDGMENTS

Thanks to Prof. Zhao Yang Li from Nankai University for measuring the ac susceptibility of complex **1**. This work was supported by the National Natural Science Foundation of China (21501093), the Natural Science Foundation of Jiangsu Province (BK20150768), and the Start up Grant from Nanjing Tech University (39837153). K.F. and T.Y. acknowledge financial support from the DFG funded transregional collaborative research centre SFB/TRR 88 “Cooperative effects in homo and heterometallic complexes (3MET)” (project A1).

REFERENCES

- (1) Thomas, L.; Lioni, F.; Ballou, R.; Gatteschi, D.; Sessoli, R.; Barbara, B. Macroscopic quantum tunnelling of magnetization in a single crystal of nanomagnets. *Nature* **1996**, *383*, 145–147.
- (2) Gatteschi, D.; Sessoli, R. Quantum tunneling of magnetization and related phenomena in molecular materials. *Angew. Chem., Int. Ed.* **2003**, *42*, 268–297.
- (3) Ding, Y. S.; Yu, K. X.; Reta, D.; Ortu, F.; Winpenny, R. E. P.; Zheng, Y. Z.; Chilton, N. F. Field and temperature dependent quantum tunnelling of the magnetisation in a large barrier single molecule magnet. *Nat. Commun.* **2018**, *9*, 3134.
- (4) Gaita Arino, A.; Luis, F.; Hill, S.; Coronado, E. Molecular spins for quantum computation. *Nat. Chem.* **2019**, *11*, 301–309.

- (5) Atzori, M.; Sessoli, R. The second quantum revolution: role and challenges of molecular chemistry. *J. Am. Chem. Soc.* **2019**, *141*, 11339–11352.
- (6) Moreno Pineda, E.; Godfrin, C.; Balestro, F.; Wernsdorfer, W.; Ruben, M. Molecular spin qubits for quantum algorithms. *Chem. Soc. Rev.* **2018**, *47*, 501–503.
- (7) Bogani, L.; Wernsdorfer, W. Molecular spintronics using single molecule magnets. *Nat. Mater.* **2008**, *7*, 179–186.
- (8) Tasiopoulos, A. J.; Vinslava, A.; Wernsdorfer, W.; Abboud, K. A.; Christou, G. Giant single molecule magnets: Giant Single Molecule Magnets: A {Mn₈₄} Torus and Its Supramolecular Nanotubes. *Angew. Chem., Int. Ed.* **2004**, *43*, 2117–2121.
- (9) Ako, A. M.; Hewitt, I. J.; Mereacre, V.; Clérac, R.; Wernsdorfer, W.; Anson, C. E.; Powell, A. K. A Ferromagnetically Coupled Mn₁₉ Aggregate with a Record S = 83/2 Ground Spin State. *Angew. Chem., Int. Ed.* **2006**, *45*, 4926–4929.
- (10) Ruiz, E.; Cirera, J.; Cano, J.; Alvarez, S.; Loose, C.; Kortus, J. Can large magnetic anisotropy and high spin really coexist? *Chem. Commun.* **2008**, 52–54.
- (11) Kang, S.; Zheng, H.; Liu, T.; Hamachi, K.; Kanegawa, S.; Sugimoto, K.; Shiota, Y.; Hayami, S.; Mito, M.; Nakamura, T.; Nakano, M.; Baker, M. L.; Nojiri, H.; Yoshizawa, K.; Duan, C.; Sato, O. A ferromagnetically coupled Fe₄₂ cyanide bridged nanocage. *Nat. Commun.* **2015**, *6*, 5955.
- (12) Ishikawa, N.; Sugita, M.; Ishikawa, T.; Koshihara, S.; Kaizu, Y. Lanthanide Double Decker Complexes Functioning as Magnets at the Single Molecular Level. *J. Am. Chem. Soc.* **2003**, *125*, 8694–8695.
- (13) Freedman, D. E.; Harman, W. H.; Harris, T. D.; Long, G. J.; Chang, C. J.; Long, J. R. Slow Magnetic Relaxation in a High Spin Iron(II) Complex. *J. Am. Chem. Soc.* **2010**, *132*, 1224–1225.
- (14) Vallejo, J.; Castro, I.; Ruiz Garcia, R.; Cano, J.; Julve, M.; Lloret, F.; De Munno, G.; Wernsdorfer, W.; Pardo, E. Field Induced Slow Magnetic Relaxation in a Six Coordinate Mononuclear Cobalt (II) Complex with a Positive Anisotropy. *J. Am. Chem. Soc.* **2012**, *134*, 15704–15707.
- (15) Guo, F. S.; Bar, A. K.; Layfield, R. A. Main Group Chemistry at the Interface with Molecular Magnetism. *Chem. Rev.* **2019**, *119*, 8479–8505.
- (16) Liu, J. L.; Chen, Y. C.; Tong, M. L. Symmetry strategies for high performance lanthanide based single molecule magnets. *Chem. Soc. Rev.* **2018**, *47*, 2431–2453.
- (17) McAdams, S. G.; Ariciu, A. M.; Kostopoulos, A. K.; Walsh, J. P. S.; Tuna, F. Molecular single ion magnets based on lanthanides and actinides: Design considerations and new advances in the context of quantum technologies. *Coord. Chem. Rev.* **2017**, *346*, 216–239.
- (18) Lu, J. J.; Guo, M.; Tang, J. K. Recent developments in lanthanide single molecule magnets. *Chem. Asian J.* **2017**, *12*, 2772–2779.
- (19) Pointillart, F.; Cador, O.; Le Guennic, B.; Ouahab, L. Uncommon lanthanide ions in purely 4f Single Molecule Magnets. *Coord. Chem. Rev.* **2017**, *346*, 150–175.
- (20) Feng, M.; Tong, M. L. Single Ion Magnets from 3d to 5f: Developments and Strategies. *Chem. Eur. J.* **2018**, *24*, 7574–7594.
- (21) Bar, A. K.; Pichon, C.; Sutter, J. P. Magnetic anisotropy in two to eight coordinated transition metal complexes: Recent developments in molecular magnetism. *Coord. Chem. Rev.* **2016**, *308*, 346–380.
- (22) Frost, J. M.; Harriman, K. L. M.; Murugesu, M. The rise of 3 d single ion magnets in molecular magnetism: towards materials from molecules? *Chem. Sci.* **2016**, *7*, 2470–2491.
- (23) Craig, G. A.; Murrie, M. 3d single ion magnets. *Chem. Soc. Rev.* **2015**, *44*, 2135–2147.
- (24) Meihaus, K. R.; Long, J. R. Actinide based single molecule magnets. *Dalton Trans.* **2015**, *44*, 2517–2528.
- (25) Goodwin, C. A. P.; Ortu, F.; Reta, D.; Chilton, N. F.; Mills, D. P. Molecular magnetic hysteresis at 60 K in dysprosocenium. *Nature* **2017**, *548*, 439–442.
- (26) Yu, K. X.; Kragoskow, J. G. C.; Ding, Y. S.; Zhai, Y. Q.; Reta, D.; Chilton, N. F.; Zheng, Y. Z. Enhancing Magnetic Hysteresis in Single Molecule Magnets by Ligand Functionalization. *Chem.* **2020**, *6*, 1777–1793.
- (27) Harriman, K. L.; Brosmer, J. L.; Ungur, L.; Diaconescu, P. L.; Murugesu, M. Pursuit of record breaking energy barriers: A study of magnetic axiality in diamide ligated Dy III single molecule magnets. *J. Am. Chem. Soc.* **2017**, *139*, 1420–1423.
- (28) Canaj, A. B.; Dey, S.; Marti, E. R.; Wilson, C.; Rajaraman, G.; Murrie, M. Insight into D_{6h} symmetry: Targeting strong axiality in stable dysprosium(III) hexagonal bipyramidal single ion magnets. *Angew. Chem., Int. Ed.* **2019**, *58*, 14146–14151.
- (29) Chen, Y. C.; Liu, J. L.; Ungur, L.; Liu, J.; Li, W.; Wang, L. F.; Ni, Z. P.; Chibotaru, F.; Chen, X. M.; Tong, M. L. Symmetry supported magnetic blocking at 20 K in pentagonal bipyramidal dy(III) single ion magnets. *J. Am. Chem. Soc.* **2016**, *138*, 2829–2837.
- (30) Yao, X. N.; Du, J. Z.; Zhang, Y. Q.; Leng, X. B.; Yang, M. W.; Jiang, S. D.; Wang, Z. X.; Ouyang, Z. W.; Deng, L.; Wang, B. W.; Gao, S. Two coordinate Co(II) imido complexes as outstanding single molecule magnets. *J. Am. Chem. Soc.* **2017**, *139*, 373–380.
- (31) Rechkemmer, Y.; Breitgoff, F. D.; van der Meer, M.; Atanasov, M.; Haki, M.; Orlita, M.; Neugebauer, P.; Neese, F.; Sarkar, B.; van Slageren, J. A four coordinate cobalt(II) single ion magnet with coercivity and a very high energy barrier. *Nat. Commun.* **2016**, *7*, 10467.
- (32) Pavlov, A. A.; Nelyubina, Y. V.; Kats, S. V.; Penkova, L. V.; Efimov, N. N.; Dmitrienko, A. O.; Vologzhanina, A. V.; Belov, A. S.; Voloshin, Y. Z.; Novikov, V. V. Polymorphism in a cobalt based single ion magnet tuning its barrier to magnetization relaxation. *J. Phys. Chem. Lett.* **2016**, *7*, 4111–4116.
- (33) Yao, B.; Singh, M. K.; Deng, Y. F.; Wang, Y. N.; Dunbar, K. R.; Zhang, Y. Z. Trigonal prismatic cobalt(II) single ion magnets: Manipulating the magnetic relaxation through symmetry control. *Inorg. Chem.* **2020**, *59*, 8505–8513.
- (34) Shi, L.; Shao, D.; Wei, H. Y.; Wang, X. Y. Two Interpenetrated Cobalt(II) Metal–Organic Frameworks with Guest Dependent Structures and Field Induced Single Ion Magnet Behaviors. *Cryst. Growth Des.* **2018**, *18*, 5270–5278.
- (35) Mondal, P.; Dey, B.; Roy, S.; Bera, S. P.; Nasani, R.; Santra, A.; Konar, S. Field Induced Slow Magnetic Relaxation and Anion/Solvent Dependent Proton Conduction in Cobalt(II) Coordination Polymers. *Cryst. Growth Des.* **2018**, *18*, 6211–6220.
- (36) Ruamps, R.; Batchelor, L. J.; Guillot, R.; Zakhia, G.; Barra, A. L.; Wernsdorfer, W.; Guihéry, N.; Mallah, T. Ising type magnetic anisotropy and single molecule magnet behaviour in mononuclear trigonal bipyramidal Co(II) complexes. *Chem. Sci.* **2014**, *5*, 3418–3424.
- (37) Guo, F. S.; Day, B. M.; Chen, Y. C.; Tong, M. L.; Mansikkamäki, A.; Layfield, R. A. Magnetic hysteresis up to 80 K in a dysprosium metallocene single molecule magnet. *Science* **2018**, *362*, 1400–1403.
- (38) Bunting, P. C.; Atanasov, M.; Damgaard Møller, E.; Perfetti, M.; Crassee, I.; Orlita, M.; Overgaard, J.; van Slageren, J.; Neese, F.; Long, J. R. A linear cobalt(II) complex with maximal orbital angular momentum from a non Aufbau ground state. *Science* **2018**, *362*, No. eaat7319.
- (39) Deng, Y. F.; Singh, M. K.; Gan, D. X.; Xiao, T.; Wang, Y.; Liu, S.; Wang, Z.; Ouyang, Z.; Zhang, Y. Z.; Dunbar, K. R. Probing the axial distortion effect on the magnetic anisotropy of octahedral Co(II) complexes. *Inorg. Chem.* **2020**, *59*, 7622–7630.
- (40) Shao, D.; Zhang, S. L.; Shi, L.; Zhang, Y. Q.; Wang, X. Y. Probing the effect of axial ligands on easy plane anisotropy of pentagonal bipyramidal cobalt(II) single ion magnets. *Inorg. Chem.* **2016**, *55*, 10859–10869.
- (41) Huang, X. C.; Li, J. X.; Chen, Y. Z.; Wang, W. Y.; Xu, R.; Tao, J. X.; Shao, D.; Zhang, Y. Q. Tuning magnetic anisotropy in a class of Co(II) bis(hexafluoroacetylacetonate) complexes. *Chem. Asian J.* **2020**, *15*, 1469–1477.
- (42) Brachnakova, B.; Matejova, S.; Moncol, J.; Herchel, R.; Pavlik, J.; Moreno Pineda, E.; Ruben, M.; Salitros, I. Stereochemistry of coordination polyhedra vs. single ion magnetism in penta and

hexacoordinated Co(II) complexes with tridentate rigid ligands. *Dalton Trans.* **2020**, *49*, 1249–1264.

(43) Mondal, A. K.; Goswami, T.; Misra, A.; Konar, S. Probing the effects of ligand field and coordination geometry on magnetic anisotropy of pentacoordinate cobalt(II) single ion magnets. *Inorg. Chem.* **2017**, *56*, 6870–6878.

(44) Zadrozny, J. M.; Telsner, J.; Long, J. R. Slow magnetic relaxation in the tetrahedral cobalt(II) complexes [Co(EPh)(4)](2) (E = O, S, Se). *Polyhedron* **2013**, *64*, 209–217.

(45) Saber, M. R.; Dunbar, K. R. Ligands effects on the magnetic anisotropy of tetrahedral cobalt complexes. *Chem. Commun.* **2014**, *50*, 12266–12269.

(46) Yao, X. N.; Yang, M. W.; Xiong, J.; Liu, J. J.; Gao, C.; Meng, Y. S.; Jiang, S. D.; Wang, B. W.; Gao, S. Enhanced magnetic anisotropy in the tellurium coordinated cobalt single ion magnet. *Inorg. Chem. Front.* **2017**, *4*, 701–705.

(47) Sarkar, A.; Tewary, S.; Sinkar, S.; Rajaraman, G. Magnetic anisotropy in (CoX₄) X II (X = O, S, Se) single ion magnets: Role of structural distortions versus heavy atom effect. *Chem. Asian J.* **2019**, *14*, 4696–4704.

(48) Sottini, S.; Poneti, G.; Ciattini, S.; Levesanos, N.; Ferentinos, E.; Krzystek, J.; Sorace, L.; Kyritsis, P. Magnetic anisotropy of tetrahedral Co(II) single ion magnets: Solid state effects. *Inorg. Chem.* **2016**, *55*, 9537–9548.

(49) Tripathi, S.; Vaidya, S.; Ansari, K. U.; Ahmed, N.; Riviere, E.; Spillecke, L.; Koo, C.; Klingeler, R.; Mallah, T.; Rajaraman, G.; Shanmugam, M. Influence of a counteranion on the zero field splitting of tetrahedral cobalt(II) Thiourea Complexes. *Inorg. Chem.* **2019**, *58*, 9085–9100.

(50) Yi, G. J.; Zhang, C. Y.; Zhao, W.; Cui, H. H.; Chen, L.; Wang, Z.; Chen, X. T.; Yuan, A.; Liu, Y. Z.; Ouyang, Z. W. Structure, magnetic anisotropy and relaxation behavior of seven coordinate Co(ii) single ion magnets perturbed by counter anions. *Dalton Trans.* **2020**, *49*, 7620–7627.

(51) Zhu, Y. Y.; Zhang, Y. Q.; Yin, T. T.; Gao, C.; Wang, B. W.; Gao, S. A family of Co^{II}Co^{III} single ion magnets with zero field slow magnetic relaxation: Fine tuning of energy barrier by remote substituent and counter cation. *Inorg. Chem.* **2015**, *54*, 5475–5486.

(52) Cui, H. H.; Lu, F.; Chen, X. T.; Zhang, Y. Q.; Tong, W.; Xue, Z. L. Zero field slow magnetic relaxation and hysteresis loop in four coordinate Co(II) single ion magnets with strong easy axis anisotropy. *Inorg. Chem.* **2019**, *58*, 12555–12564.

(53) Ziegenbalg, S.; Hornig, D.; Gorls, H.; Plass, W. Cobalt(ii) based single ion magnets with distorted pseudotetrahedral [N₂O₂] coordination: Experimental and theoretical investigations. *Inorg. Chem.* **2016**, *55*, 4047–4058.

(54) Wu, T.; Zhai, Y. Q.; Deng, Y. F.; Chen, W. P.; Zhang, T.; Zheng, Y. Z. Correlating magnetic anisotropy with the subtle coordination geometry variation of a series of cobalt(ii) sulfonamide complexes. *Dalton Trans.* **2019**, *48*, 15419–15426.

(55) Peng, Y.; Mereacre, V.; Anson, C. E.; Zhang, Y.; Bodenstein, T.; Fink, K.; Powell, A. K. Field Induced Co(II) Single Ion Magnets with mer Directing Ligands but Ambiguous Coordination Geometry. *Inorg. Chem.* **2017**, *56*, 6056–6066.

(56) Wu, Y.; Tian, D.; Ferrando Soria, J.; Cano, J.; Yin, L.; Ouyang, Z.; Wang, Z.; Luo, S.; Liu, X.; Pardo, E. Modulation of the magnetic anisotropy of octahedral cobalt(ii) single ion magnets by fine tuning the axial coordination microenvironment. *Inorg. Chem. Front.* **2019**, *6*, 848–856.

(57) Vaidya, S.; Shukla, P.; Tripathi, S.; Riviere, E.; Mallah, T.; Rajaraman, G.; Shanmugam, M. Substituted versus Naked Thiourea Ligand Containing Pseudotetrahedral Cobalt(II) Complexes: A Comparative Study on Its Magnetization Relaxation Dynamics Phenomenon. *Inorg. Chem.* **2018**, *57*, 3371–3386.

(58) Vallejo, J.; Viciano Chumillas, M.; Lloret, F.; Julve, M.; Castro, I.; Krzystek, J.; Ozerov, M.; Armentano, D.; De Munno, G.; Cano, J. Coligand Effects on the Field Induced Double Slow Magnetic Relaxation in Six Coordinate Cobalt(II) Single Ion Magnets (SIMs)

with Positive Magnetic Anisotropy. *Inorg. Chem.* **2019**, *58*, 15726–15740.

(59) Palion Gazda, J.; Choroba, K.; Machura, B.; Switlicka, A.; Kruszynski, R.; Cano, J.; Lloret, F.; Julve, M. Influence of the pyrazine substituent on the structure and magnetic properties of dicyanamide bridged cobalt(ii) complexes. *Dalton Trans.* **2019**, *48*, 17266–17280.

(60) Peng, G.; Chen, Y.; Li, B.; Zhang, Y. Q.; Ren, X. M. Bulky Schiff base ligand supported Co(II) single ion magnets with zero field slow magnetic relaxation. *Dalton Trans.* **2020**, *49*, 5798–5802.

(61) TURBOMOLE, V7.2; TURBOMOLE GmbH: Karlsruhe, Germany, 2017.

(62) Meier, U.; Staemmler, V. AN EFFICIENT 1ST ORDER CASSCF METHOD BASED ON THE RENORMALIZED FOCK OPERATOR TECHNIQUE. *Theor. Chim. Acta.* **1989**, *76*, 95–111.

(63) Bodenstein, T. *Entwicklung und Anwendung von Multi referenzverfahren zur Beschreibung magnetischer Eigenschaften von Metallkomplexen*. Dissertation, Karlsruher Institut für Technologie (KIT), Karlsruhe, Germany, 2015.

(64) Software developed in Kaiserslautern and Karlsruhe in the collaborative research center TRR88 ‘3MET’.

(65) Neese, F. Efficient and accurate approximations to the molecular spin orbit coupling operator and their use in molecular g tensor calculations. *J. Chem. Phys.* **2005**, *122*, 034107.

(66) Helmich Paris, B.; Hättig, C.; van Wüllen, C. Spin Free CC2 Implementation of Induced Transitions between Singlet Ground and Triplet Excited States. *J. Chem. Theory Comput.* **2016**, *12*, 1892–1904.

(67) Gerloch, M.; McMeeking, R. F. Paramagnetic properties of unsymmetrical transition metal complexes. *J. Chem. Soc., Dalton Trans.* **1975**, *22*, 2443–2451.

(68) Sheldrick, G. M. SHELXT Integrated space group and crystal structure determination. *Acta Crystallogr., Sect. C: Struct. Chem.* **2015**, *71*, 3–8.

(69) Cazaux, J. B.; Braunstein, P.; Magna, L.; Saussine, L.; Olivier Bourbigou, H. Mono(aryloxo)Titanium(IV) Complexes and Their Application in the Selective Dimerization of Ethylene. *Eur. J. Inorg. Chem.* **2009**, *2009*, 2942–2950.

(70) Jiao, G.; Tao, T.; Ke Hua, G.; Gang, W.; Wei, H. Two air oxidation copper(II) complexes of salicylaldehyde derivatives obtained by in situ copper(II) ion catalysis and complexation. *Inorg. Chem. Commun.* **2011**, *14*, 1978–1981.

(71) Pinsky, M.; Avnir, D. Continuous symmetry measures S. The classical polyhedral. *Inorg. Chem.* **1998**, *37*, 5575–5582.

(72) Casanova, D.; Cirera, J.; Lluell, M.; Alemany, P.; Avnir, D.; Alvarez, S. Minimal distortion pathways in polyhedral rearrangements. *J. Am. Chem. Soc.* **2004**, *126*, 1755–1763.

(73) Titiš, J.; Boča, R. Magnetostructural D Correlations in Hexacoordinated Cobalt(II) Complexes. *Inorg. Chem.* **2011**, *50*, 11838–11845.

(74) Chilton, N. F.; Anderson, R. P.; Turner, L. D.; Soncini, A.; Murray, K. S. PHI: A powerful new program for the analysis of anisotropic monomeric and exchange coupled polynuclear d and f block complexes. *J. Comput. Chem.* **2013**, *34*, 1164–1175.

(75) Zhang, J.; Li, J.; Yang, L.; Yuan, C.; Zhang, Y. Q.; Song, Y. Magnetic Anisotropy from Trigonal Prismatic to Trigonal Anti prismatic Co(II) Complexes: Experimental Observation and Theoretical Prediction. *Inorg. Chem.* **2018**, *57*, 3903–3912.

(76) Rodríguez Diéguez, A.; Pérez Yáñez, S.; Ruiz Rubio, L.; Seco, J. M.; Cepeda, J. From isolated to 2D coordination polymers based on 6 aminonicotinate and 3d metal ions: towards field induced single ion magnets. *CrystEngComm* **2017**, *19*, 2229–2242.

(77) Goswami, S.; Leitus, G.; Tripuramallu, B. K.; Goldberg, I. MnII and CoII Coordination Polymers Showing Field Dependent Magnetism and Slow Magnetic Relaxation Behavior. *Cryst. Growth Des.* **2017**, *17*, 4393–4404.

(78) Reta, D.; Chilton, N. F. Uncertainty estimates for magnetic relaxation times and magnetic relaxation parameters. *Phys. Chem. Chem. Phys.* **2019**, *21*, 23567–23575.

(79) Shrivastava, K. N. Theory of Spin Lattice Relaxation. *Phys. Status Solidi B* **1983**, *117*, 437–458.

(80) Singh, A.; Shrivastava, K. N. Optical Acoustic Two Phonon Relaxation in Spin Systems. *Phys. Status Solidi B* **1979**, *95*, 273–277.

(81) Liu, J.; Chen, Y. C.; Liu, J. L.; Vieru, V.; Ungur, L.; Jia, J. H.; Chibotaru, L. F.; Lan, Y.; Wernsdorfer, W.; Gao, S.; Chen, X. M.; Tong, M. L. A Stable Pentagonal Bipyramidal Dy(III) Single Ion Magnet with a Record Magnetization Reversal Barrier over 1000 K. *J. Am. Chem. Soc.* **2016**, *138*, 5441–5450.

(82) Gomez Coca, S.; Urtizberea, A.; Cremades, E.; Alonso, P. J.; Camon, A.; Ruiz, E.; Luis, F. Origin of slow magnetic relaxation in Kramers ions with non uniaxial anisotropy. *Nat. Commun.* **2014**, *5*, 4300.

(83) Korchagin, D. V.; Pali, A. V.; Yureva, E. A.; Akimov, A. V.; Misochko, E. Y.; Shilov, G. V.; Talantsev, A. D.; Morgunov, R. B.; Shakin, A. A.; Aldoshin, S. M.; Tsukerblat, B. S. Evidence of field induced slow magnetic relaxation in cis [Co(hfac)(2)(H₂O)(2)] exhibiting tri axial anisotropy with a negative axial component. *Dalton Trans.* **2017**, *46*, 7540–7548.

(84) Diaz Torres, R.; Menelaou, M.; Roubeau, O.; Sorrenti, A.; Brandariz De Pedro, G.; Sanudo, E. C.; Teat, S. J.; Fraxedas, J.; Ruiz, E.; Aliaga Alcalde, N. Multiscale study of mononuclear Co II SMMs based on curcuminoid ligands. *Chem. Sci.* **2016**, *7*, 2793–2803.

(85) Vaidya, S.; Upadhyay, A.; Singh, S. K.; Gupta, T.; Tewary, S.; Langley, S. K.; Walsh, J. P.; Murray, K. S.; Rajaraman, G.; Shanmugam, M. A synthetic strategy for switching the single ion anisotropy in tetrahedral Co(II) complexes. *Chem. Commun.* **2015**, *51*, 3739–3742.

(86) Chen, L.; Zhou, J.; Cui, H. H.; Yuan, A. H.; Wang, Z.; Zhang, Y. Q.; Ouyang, Z. W.; Song, Y. Slow magnetic relaxation influenced by change of symmetry from ideal C_{4v} to D_{3d} in cobalt(II) based single ion magnets. *Dalton Trans.* **2018**, *47*, 2506–2510.

(87) Roy, S.; Oyarzabal, I.; Vallejo, J.; Cano, J.; Colacio, E.; Bauza, A.; Frontera, A.; Kirillov, A. M.; Drew, M. G.; Das, S. Two Polymorphic Forms of a Six Coordinate Mononuclear Cobalt(II) Complex with Easy Plane Anisotropy: Structural Features, Theoretical Calculations, and Field Induced Slow Relaxation of the Magnetization. *Inorg. Chem.* **2016**, *55*, 8502–8513.

(88) Hu, Z. B.; Jing, Z. Y.; Li, M. M.; Yin, L.; Gao, Y. D.; Yu, F.; Hu, T. P.; Wang, Z.; Song, Y. Important Role of Intermolecular Interaction in Cobalt(II) Single Ion Magnet from Single Slow Relaxation to Double Slow Relaxation. *Inorg. Chem.* **2018**, *57*, 10761–10767.

(89) Ho, L. T. A.; Chibotaru, L. F. Intermolecular mechanism for multiple maxima in molecular dynamic susceptibility. *Phys. Rev. B: Condens. Matter Mater. Phys.* **2018**, *98*, 174418.

(90) Shao, D.; Shi, L.; Yin, L.; Wang, B. L.; Wang, Z. X.; Zhang, Y. Q.; Wang, X. Y. Reversible on off switching of both spin crossover and single molecule magnet behaviours via a crystal to crystal transformation. *Chem. Sci.* **2018**, *9*, 7986–7991.

(91) Rigamonti, L.; Bridonneau, N.; Poneti, G.; Tesi, L.; Sorace, L.; Pinkowicz, D.; Jover, J.; Ruiz, E.; Sessoli, R.; Cornia, A. A Pseudo Octahedral Cobalt(II) Complex with Bispyrazolylpyridine Ligands Acting as a Zero Field Single Molecule Magnet with Easy Axis Anisotropy. *Chem. Eur. J.* **2018**, *24*, 8857–8868.